Mineralogical Magazine, June 2004, Vol. 68(3), pp. 455–465

Assessment of the use of Raman spectroscopy for the determination of amphibole asbestos

C. RINAUDO[1], E. BELLUSO[2] AND D. GASTALDI[1]

[1] Dipartimento di Scienze dell'Ambiente e della Vita, Università del Piemonte Orientale 'Amedeo Avogadro', Piazza Ambrosoli 5, 15100 Alessandria, Italy
[2] Dipartimento di Scienze Mineralogiche e Petrologiche, Università di Torino, Via Valperga Caluso 35, 10125 Torino, Italy

ABSTRACT

Raman spectroscopy was assessed for its ability to rapidly identify asbestos phases by submitting the amphiboles anthophyllite, amosite, crocidolite and tremolite to spectroscopic analysis. All the phases were characterized by using XRD, SEM, TEM (CTEM, SAED), AEM and EDS techniques. This study demonstrates that accurate identification of the mineralogical phase can be attained by analysing the position in the Raman spectrum of the bands corresponding to the symmetric stretching modes (ν_s) and to the antisymmetric stretching modes (ν_{as}) of the different Si–O linkages. Raman spectroscopy thus proves to be an effective technique for rapidly distinguishing the different fibrous minerals examined.

KEYWORDS: Raman spectroscopy, transmission electron microscopy, asbestos.

Introduction

THE term 'asbestos' refers to a family of fibrous minerals belonging to the serpentine group (chrysotile) and to the amphibole group (actinolite, anthophyllite, amosite, crocidolite and tremolite). Used mainly in the building industry, these minerals have deleterious effects on the human body. The resultant damage is dependent upon a combination of factors such as length of exposure, individual sensitivity and the nature of the material that has been inhaled. Experimental techniques for the detection of asbestos fibres and for the identification of the mineralogical species present in a given sample are therefore of great interest. Of the techniques currently available, Raman spectroscopy has several clear advantages: it is extremely simple to perform, requires no specimen preparation and, when used in conjunction with a microscope, allows the spectrum from a bundle of fibres to be obtained. Several reports in the literature have dealt with Raman characterization of different species of asbestos while using a microspectrometer, and the Raman spectra obtained from selected micrometric bundles of fibres: Blaha and Rosasco (1978); Lewis *et al*. (1996); Bard *et al*. (1997); Kloprogge *et al*. (1999). At first glance, comparison of the results obtained on the same mineralogical phase by the different authors reveals various discrepancies. However, no information is reported, in the works cited, about the chemical composition of the minerals analysed, leaving a margin of doubt about conclusions based on these apparent discrepancies.

In order to contribute to the determination of the Raman spectrum of an asbestos phase with a well-defined chemical composition, we applied Raman analysis to fibrous samples previously characterized chemically and mineralogically using X-ray powder diffraction (XRD), scanning electron microscopy (SEM), transmission electron microscopy (TEM) coupled with EDS (energy dispersion spectrometry) and analytical electron microscopy (AEM). In a previous work by the present authors (Rinaudo *et al*., 2003) the serpentine asbestos (chrysotile) was characterized from crystallographic and spectroscopic points of

* E-mail: caterina.rinaudo@unipmn.it
DOI: 10.1180/0026461046830197

view: in this paper we describe the Raman spectra obtained from amosite, anthophyllite, crocidolite and tremolite, and show that Raman spectroscopy can be used for the identification of the studied phases. Actinolite was not included in the study, for chemical and mineralogical characterization of all the actinolite samples from different sources revealed them actually to be tremolite.

Experimental

Samples of the materials studied were obtained from private collections, from the Azienda Ospedaliera SS. Antonio e Biagio, Alessandria (Italy) and from the Museo Regionale di Scienze Naturali of Torino (Italy).

Each sample was first examined by XRD with the powder method, using a Siemens D5000 diffractometer equipped with Cu-$K\alpha$ radiation. Samples pure enough from a mineralogical point of view, i.e. those for which the XRD spectrum showed a large preponderance of one asbestos phase and small amounts of other mineralogical phases, underwent further characterization.

Morphological study and basic chemical analysis of the selected samples were performed using a Cambridge Stereoscan 360 SEM equipped with a Link Oxford Pentafet ATW2 analytical energy dispersive microanalysis system (EDS).

The chemical compositions of the different samples were determined using transmission electron microscopy (TEM) by selected area electron diffraction (SAED), with observations made at medium (CTEM – conventional transmission electron microscopy) and sometimes high magnification (HRTEM), and by analytical electron microscopy (AEM). Both TEM and AEM analyses were performed using a Philips CM12 TEM, working at 120 kV, and equipped with an EDAX Si (Li) detector, and processed with a PV9900 system for energy dispersive microanalyses. The AEM analyses were performed on isolated fibres. The data were processed with the SUPQ software using default K factors. The different samples of amphibole asbestos were classified according to Leake *et al*. (1997) using the NEWAMPHCAL program written by Yavuz (1999). On the basis of the chemical composition determined by EDS, NEWAMPHCAL calculates a structural amphibole formula allocating Fe, detected as Fe^{2+} by EDS, to Fe^{2+} and Fe^{3+} on the basis of a procedure proposed by Droop (1987). Water was not detected, so the data were normalized to 23 oxygen atoms.

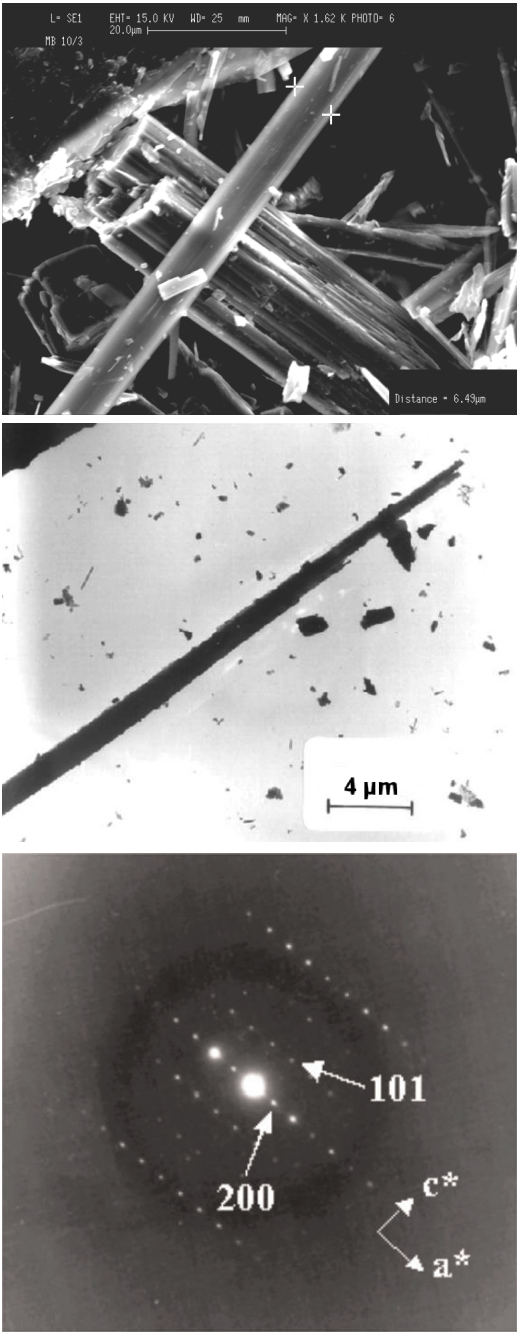

FIG. 1. (*a*) Secondary electron SEM image of the anthophyllite sample studied. (*b*) TEM image of an anthophyllite fibre; at the top of the fibre, thin fibrils can be seen splitting off the sample. (*c*) Diffraction pattern from the fibre shown in Fig. 1*a* and observed along [010]. The fibre axis runs along the [001] direction.

Finally, the different asbestos phases were studied under a Jobin Yvon HR800 LabRam μ-spectrometer equipped with an Olympus BX41 microscope, an HeNe 20 mW laser working at 632.8 nm and a CCD air-cooled detector. In order to balance the signal against noise, 10 cycles of 100 scans were performed.

In this work, only the Raman region corresponding to 1200–150 cm^{-1} was analysed.

Anthophyllite

The samples selected for detailed characterization of the anthophyllite phase came from the Bresimo Mine (near Trento, Trentino Alto Adige, Italy). Observed under SEM (Fig. 1*a*) the samples appear as bundles of stiff fibres with a prismatic habit. The splitting of thick fibres into finer and therefore more flexible fibrils can be seen in the SEM and TEM images (Fig. 1*a*,*b*), from which the fibres can be estimated to have widths ranging from 3000 to 13,000 Å.

Certain identification of the anthophyllite phase is obtained by TEM from the symmetry and the d_{hkl} values in the diffraction patterns (Fig. 1*b*,*c*) and from AEM analyses performed on several fibres which reveal a cummingtonite/anthophyllite phase (Table 1) (theoretical formula $(Mg,Fe^{2+})_7[Si_8O_{22}](OH)_2$).

A Raman spectrum registered on the fibres characterized according to their chemical and mineralogical aspects is shown in Fig. 2. The bands are identified on the basis of the description of the vibrational bands in the IR spectra of the phyllosilicates proposed by Lazarev (1972) and Farmer (1974) as well as the assignation proposed by Kloprogge *et al*. (2001) for the Raman bands of holmquistite, a Li-bearing amphibole.

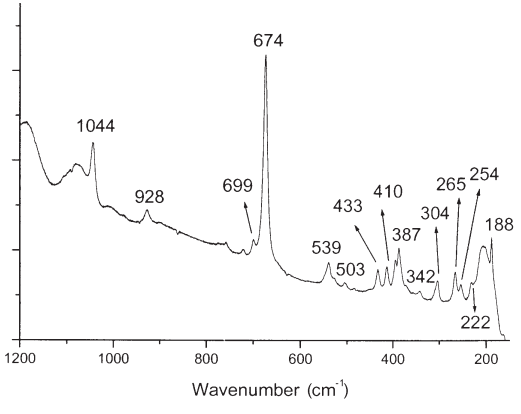

FIG. 2. A Raman spectrum registered on anthophyllite fibres such as those represented in Fig. 1*a*.

In the 1200–600 cm^{-1} spectral region, four significantly intense bands can be observed at 1044, 928, 699 and 674 cm^{-1}, regardless of the angle of the fibre to the incident beam. As described by Lazarev (1972) and Kloprogge *et al*. (2001) four Si–O_b–Si and four O–Si–O antisymmetric stretching vibrations can be observed in amphiboles in the 1150–950 cm^{-1} range. More specifically, vibrations >1000 cm^{-1} are ascribed to the antisymmetric stretching vibrations (ν_{as}) of the Si–O_b–Si linkages – in the anthophyllite spectrum this corresponds to the band observed at 1044 cm^{-1}. Instead, the bands in the 1000–950 cm^{-1} range of amphibole spectra are assigned to the ν_{as} vibrations of the O–SiO– groups; anthophyllite, however, contains no bands in this region. Following the same authors, the band at 928 cm^{-1} may be ascribed to the symmetric stretching modes (ν_s) of the O–SiO– linkages; and finally, the bands in the 750–650 cm^{-1} spectral region are produced by symmetric stretching vibrations –ν_s– of the Si–O_b–Si groups. Of the two bands detected in this region in the anthophyllite spectrum, the more intense one, which appears at 674 cm^{-1}, is ascribed to the ν_1 (A_g) symmetric stretching modes of the Si–O_b–Si bridges. In the 500–180 cm^{-1} region of the spectrum, the coupling of vibrations involving different cations, translation and libration modes of the hydroxyls and deformation modes of the $(Si_4O_{11})_\infty$ ribbons makes precise assignment of the bands problematic. Nevertheless, in the Raman spectra of minerals containing OH^- in the tetrahedral rings, in particular on phyllosilicates, vibrations produced by the groups O–H–O (wherein O's are the apical oxygens of the SiO_4 tetrahedra and H is the hydrogen of the OH group) are always observed in the 200–300 cm^{-1} range (Frost, 1995, 1997; Frost & Kristof, 1997; Rinaudo *et al*., 2003). As a consequence of the presence of OH^- in the centre of the $(Si_4O_{11})_\infty$ ribbons, vibrations in the same frequency range may be expected in amphiboles; we therefore suggest that the bands observed at 222, 254 and 265 cm^{-1} be assigned to vibrations of the O–H–O groups.

Table 2 shows the position of the bands detected on all the anthophyllite spectra (including those observed on spectra registered on fibres at different angles to the incident beam from that in Fig. 2) and compares them with the

TABLE 1. Cations from AEM analyses of different fibres from asbestos phases. The data were normalized to 23 O atoms. *M* = average of analyses; tot. cat.: total cations; oct.: octahedral. The last seven lines indicate the site occupancies and the ratios calculated by the program for amphibole asbestos classification indicated in the text.

	Anthophyllite							Tremolite						Crocidolite						Amosite						
	*A*1	*A*2	*A*3	*A*4	*A*5	*A*6	*M*	*T*1	*T*2	*T*3	*T*4	*T*5	*M*	*C*1	*C*2	*C*3	*C*4	*C*5	*M*	*AM*1	*AM*2	*AM*3	*AM*4	*AM*5	*AM*6	*M*
Si^{4+}	8	8	8	8	8	8	8	7.97	8	8	8	8	8	8	8	8	8	8	8	8	8	8	8	8	8	8
^{IV}Al	0	0	0	0	0	0	0	0.03	0	0	0	0	0	0	0	0	0	0	0	0	0	0	0	0	0	0
^{VI}Al	0.04	0	0.04	0.12	0.07	0.02	0.05	0.15	0.19	0.17	0.2	0.2	0.18	0.05	0.05	0.04	0.06	0.04	0.05	0.24	0.21	0.23	0.27	0.19	0.18	0.22
Fe^{3+}														0.64	0.75	0.71	0.64	0.61	0.67							
Fe^{2+}	0.73	0.83	0.78	0.2	1.07	0.89	0.75	0.26	0.31	0.23	0.28	0.25	0.27	3.2	3.24	3.24	3.18	3.23	3.22	4.14	4.57	4.41	4.06	4.51	4.63	4.39
Mn^{2+}	0	0	0	0	0	0.03	0	0.02	0.03	0.01	0.01	0.01	0.02							0.06	0.06	0.06	0.06	0.06	0.06	0.06
Mg^{2+}	5.96	5.75	5.67	6.08	5.55	5.76	5.8	4.74	4.7	4.47	4.45	4.73	4.62	0.4	0.29	0.36	0.56	0.41	0.4	1.71	1.53	1.79	1.74	1.62	1.58	1.66
Ca^{2+}	0	0	0	0	0.11	0	0.02	1.77	1.52	1.53	1.92	1.57	1.66	0.04	0.05	0.03	0.02	0.09	0.05							
Na^{+}														1.8	1.76	1.89	2.12	1.76	1.87							
Tot. cat.	14.73	14.58	14.49	14.4	14.8	14.7	14.62	14.94	14.75	14.41	14.86	14.76	14.75	14.13	14.14	14.27	14.58	14.14	14.26	14.15	14.37	14.49	14.13	14.38	14.44	14.33
Tot. oct. cat.																										
$(Na)_B$	0	0	0	0	0	0		0	0	0	0	0		1.8	1.76	1.89	1.98	1.76		0	0	0	0	0	0	
$(Na+K)_A$	0	0	0	0	0	0		0	0	0	0	0		0	0	0	0.14	0		0	0	0	0	0	0	
$(Ca)_B$	0	0	0	0	0.11	0		1.77	1.52	1.53	1.92	1.57		0.04	0.05	0.03	0.02	0.09		0	0	0	0	0	0	
$(Ca+Na)_B$	0	0	0	0	0.11	0		1.77	1.52	1.53	1.92	1.57		1.84	1.81	1.92	2	1.85		0	0	0	0	0	0	
Mg/(Mg+Mn)	1	1	1	1	1	1		1	0.99	1	1	1		1	1	1	1	1		0.97	0.96	0.97	0.97	0.97	0.96	
$(Mg+Fe^{2+}+Mn)$	6.69	6.59	6.46	6.29	6.62	6.68		5.02	5.04	4.71	4.74	5		3.6	3.53	3.6	3.73	3.64		5.91	6.16	6.25	5.86	6.19	6.27	
$Mg/(Mg+Fe^{2+})$	0.89	0.87	0.88	0.97	0.84	0.87		0.95	0.94	0.95	0.94	0.95		0.11	0.08	0.1	0.15	0.11		0.29	0.25	0.29	0.3	0.26	0.25	

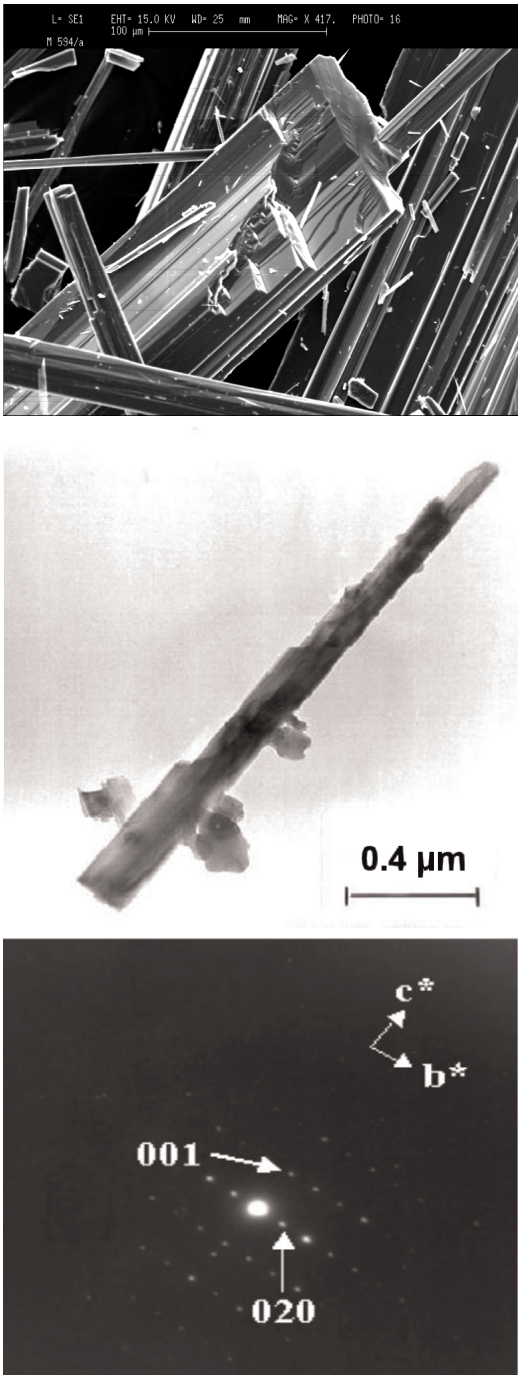

FIG. 3. (*a*) Secondary electron SEM image of the tremolite sample studied. (*b*) CTEM image of a tremolite fibre. (*c*) SAED pattern of the fibre in Fig. 3*b* and observed along [100].

results from Bard *et al*. (1997). We detected a larger number of bands, thanks to the high resolution of the instrument used; nevertheless, the band positions observed correspond well to those of Bard *et al*. (1997), and discrepancies in intensity are probably related to the different orientation of the samples in the two studies.

Tremolite

The samples of tremolite selected for study are from Brachiello (Val d'Ala, Piedmont region, Italy). The SEM observations (Fig. 3*a*) reveal them to be aggregates of very long fibres with diameters ranging from 10,000 to 15,000 Å, and thicker crystals ranging in diameter from 150,0000 to 200,0000 Å. A CTEM analysis of the fibres reveals a diffraction pattern (Fig. 3*b*,*c*) indicating 0*kl* lattice planes (d_{001} = 5.1 Å; d_{020} = 9.0 Å) and a fibre axis running in the [001] direction. The AEM analyses performed on different fibres (Table 1) indicate an homogeneous chemical composition corresponding to the tremolite phase with the theoretical formula: $Ca_2(Mg,Fe^{2+})_5[Si_8O_{22}](OH)_2$.

Figure 4 shows a Raman spectrum registered on a previously characterized fibre, analogous to those represented in Fig. 3*a*. In the spectral region 1200–600 cm^{-1}, four significantly intense bands at 1062, 1031, 932 and 676 cm^{-1}, and two weak bands at 950 and 751 cm^{-1} can be observed, regardless of the orientation of the fibre with respect to the incident beam. A very weak band appears at 740 cm^{-1} in the spectra registered with the fibre at a different angle from that in Fig. 4. As discussed for anthophyllite, according to Lazarev (1972) and Kloprogge *et al*. (2001), the bands at 1062 and 1031 cm^{-1} may be ascribed to

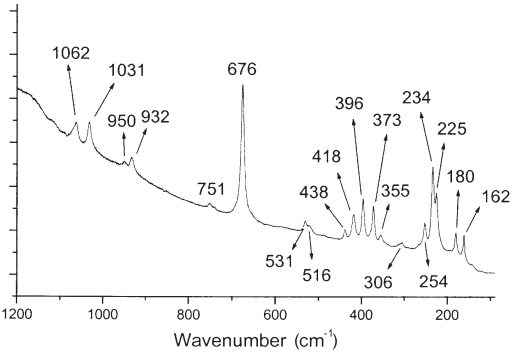

FIG. 4. A Raman spectrum of the tremolite sample represented in Fig. 3*a*.

TABLE 2. Comparison of the Raman spectra obtained by us and by other authors using different excitation wavelengths: 785 nm (Lewis *et al*., 1996); 632.8 (Bard *et al*., 1997); 514 nm (Blaha and Rosasco, 1978). [m: medium; s: strong; sh: shoulder; v: very; w: weak].

Anthophyllite This work	Anthophyllite Bard *et al*. (1997)	Tremolite This work	Tremolite Lewis *et al*. (1996)	Tremolite Bard *et al*. (1997)	Tremolite Blaha and Rosasco (1978)	Amosite This work	Amosite Lewis *et al*. (1996)	Amosite Bard *et al*. (1997)	Crocidolite This work	Crocidolite Lewis *et al*. (1996)	Crocidolite Bard *et al*. (1997)
						1093 vw		1093 vw			
									1082 s	1082 w	1085 s
		1062 m		1061 m	1061 m						
1044 s	1042 m		1044 w								
		1031 m		1028 m	1030 m				1030 w	1034 vw	1032 m
						1020 s	1016 m	1020 s			
							996 w, sh			986 w,sh	
						968 m	966 w	968 m	967 vs	971 m	969 vs
		950 w			947 w						
928 w		932 m		928 w	931 m						
						904 vw	906 w	903 vw			
									889 m	888 vw	891 s
									771 w	776 vw	772 m
		751 w			751 m						
		740 w			741 m				733 w	736 vw	737 m
699 w											
674 vs	671 vs	676 vs	677 s	672 vs	676 vs						
					670 sh						
						659 vs	657 s	658 vs	664 s	667 w	664 s
									577 s	581 m	577 vs
							556 w, sh	555 vw			
539 m									537 m	542 s	539 vs
		531 w			531 m	528 m	527 m	528 m			
		516 w			516 m						
503 vw						507 w	506 w, sh	506 w	506 w	506 w,sh	509 w
							462 w		470 w	472 w	469 m
433 m	430 m	438 w	428 m		439 m	423 w	422 w	421 m	428 m	432 w	
410 m	410 w	418 m		414 w	418 m						
		396 s		393 m	398 s	400 w	397 w	401 m			
387 m	384 m		383 m							387 w,sh	
		373 m			376 m				374 s		374 vs
364 w	362 m			369 m		368 w	367 w	364 m	360 sh	364 m	

		355 vw			355 m							
342 vw		348 vw		349 vw	348 m	348 m	347 m	349 m				
	336 vw	335 vw	338 m		335 m				331 m	331 m	332 m	
										324 m		
304 m	304 m	306 w			307 w	307 vw	312 w	309 w				
		290 w	299 m		295 w				300 m	300 m	297 s	
						289 vw	282 w	287 w				
265 m	260		261 m		268 m				272 m	272 w	271	
										260 w,sh		
254 w		254 m	248 w	251 w	254 m	252 w	252 w		246 m	253 m	249 s	
		234 s		232 w	235 s							
222 vw		225 s		222 w	226 s							
					216 s	216 m	212 m		211 m	214 vw,sh		
					196 w				195 s			
188 m		180 s			182 s	182 vs						
		162 s			164 s	155 s			162 vs			

the antisymmetric stretching vibrations $-\nu_{as}-$ of the $Si-O_b-Si$; the band at 950 cm^{-1} to $O-SiO-$; the band at 932 cm^{-1} to the symmetric stretching modes of the $O-SiO-$ linkages; lastly, the bands in the spectral region 750–650 cm^{-1} are produced by the symmetric stretching vibrations $-\nu_s-$ of the $Si-O_b-Si$ groups. Of the three bands detected in this region, the most intense, which appears at 676 cm^{-1}, is ascribed to the ν_1 (A_g) symmetric stretching modes of the $Si-O_b-Si$ bridges. In the <650 cm^{-1} region of the spectrum, as in the case of anthophyllite, assignment of the bands to the vibrational modes is problematic. Nevertheless, four bands appear in the spectral region 200–300 cm^{-1}, where we would expect to see vibrations produced by O–H–O groups: two are of weak intensity at 290 and 254 cm^{-1}, and two are of higher intensity at 234 and 225 cm^{-1}. Given that the octahedral positions on tremolite are normally occupied by two types of cations (Mg and Fe^{2+}) linked to OH^- groups (in our sample, substitutions of Al for Mg or Fe^{2+} are detected by AEM analyses, Table 1) and that the cubic sites are occupied by Ca, the presence of more than one type of O–H–O group vibrating at very similar, but not identical, frequencies is not surprising.

In Table 2 our spectrum is compared with the spectra obtained for tremolite samples by different authors using different excitation wavelengths: 514 nm, Blaha and Rosasco (1978); 785 nm, Lewis *et al*. (1996); 632.8 nm, Bard *et al*. (1997).

Our data appear to match closely those of Blaha and Rosasco (1978), with the exception of some variations in the spectral region corresponding to very low frequencies, near 200 cm^{-1}. In this region of the spectrum, vibrational modes of the cations with octahedral (*M*1, *M*2, *M*3) and cubic (*M*4) coordination are observed. We therefore hypothesize that our samples and those of Blaha and Rosasco (1978) include chemical differences in these reticular positions, although lack of specification of the sample in the latter study precludes definitive confirmation of this theory.

Table 2 also shows significant discrepancies between our spectrum and the results from Lewis *et al*. (1996), which more closely resemble those we registered on the anthophyllite phase. Since the chemical and crystallographic characteristics of the sample studied by Lewis *et al*. (1996) are not indicated, and since the anthophyllite phase is not taken into consideration, we are inclined to believe that the mineralogical phase studied in that case was anthophyllite and not actually tremolite.

Amosite

The samples of amosite (the commercial name for one member of the cummingtonite–grunerite series) characterized in the present work are from South Africa. Analysis by SEM revealed them to be made up of rather stiff bundles of fibres measuring in some cases up to several cm long (Fig. 5*a*). The XRD and AEM analyses (Table 1) confirm the homogeneity of the whole sample and allow it to be classified as grunerite–ferroanthophyllite (theoretical formula: $(Fe^{2+},Mg)_7[Si_8O_{22}](OH)_2$). The widths of the individual fibres, measured on the images obtained by CTEM, range from 1500 to 4800 Å (Fig. 5*b*). The d_{hkl} values calculated from the SAED images (Fig. 5*c*) indicate 0*kl* lattice planes and an elongation axis of the fibres parallel to the [001] direction.

The spectrum registered on fibres such as those represented in Fig. 5*a* is shown in Fig. 6. The most intense band at 659 cm^{-1} is assigned to ν_s of the Si−O_b−Si linkages, as in the case of anthophyllite and tremolite. The bands at 1020 and 968 cm^{-1} may be assigned, according to Lazarev (1972), to ν_{as} of the Si−O−Si bridges, and to ν_{as} of the O−SiO− linkages, respectively, while the band at 904 cm^{-1} may be assigned to ν_s of the O−SiO− linkages (Lewis *et al*., 1996). In the spectral region where vibrations of O−H−O groups are expected, only three bands are observed, at 289, 252 and 216 cm^{-1}.

Table 2 allows comparison of our spectra with those reported by Lewis *et al*. (1996) and by Bard *et al*. (1997), showing a good match in every case.

Crocidolite

The samples of the 'blue' asbestos studied in the present work are from South Africa. Analysis by SEM reveals the samples to be made up of very long, fine, flexible fibres, ranging from 500 to 2000 Å wide (Fig. 7*a*). Diffraction patterns of the fibres (Fig. 7*b*,*c*) indicate *h*0*l* lattice planes and an elongation axis of the fibres parallel to the [001] direction; the presence of 0*kl* streaked spots (Fig. 7*c*) indicate that the samples are rich in chain-wide faults. The AEM analyses (Table 1)

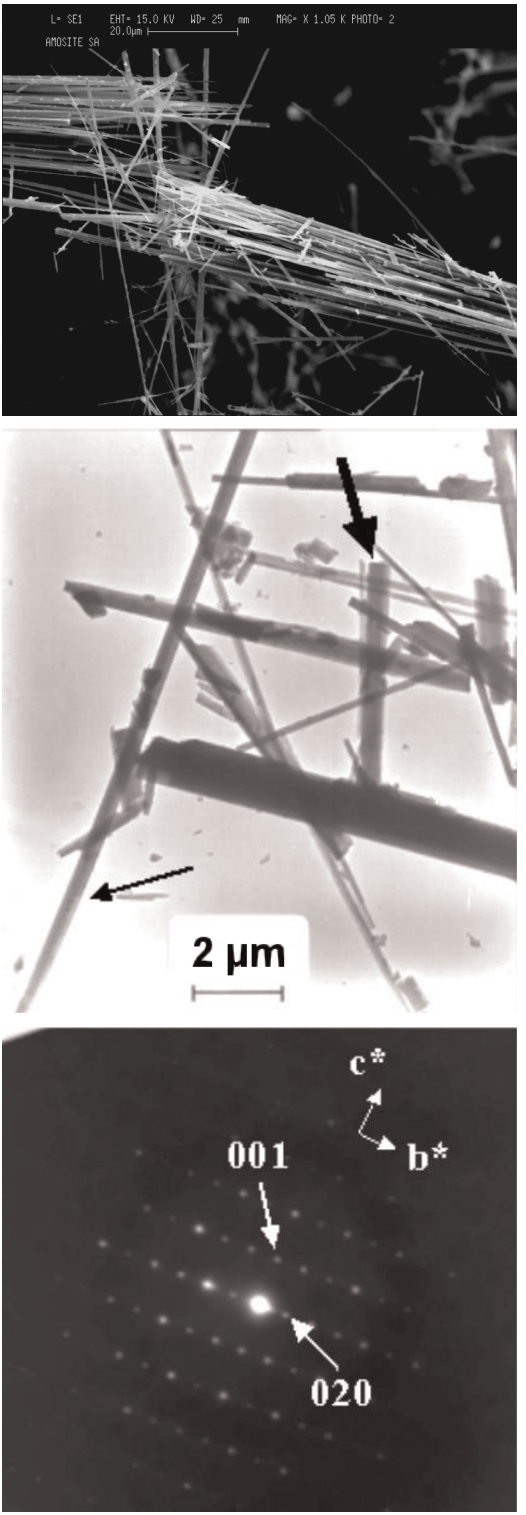

FIG. 5. (*a*) Secondary electron SEM image of the amosite sample studied. (*b*) CTEM image: the thick arrow indicates an instance of fibril splitting. (*c*) SAED pattern from the fibre indicated by the thin arrow in Fig. 5*b*.

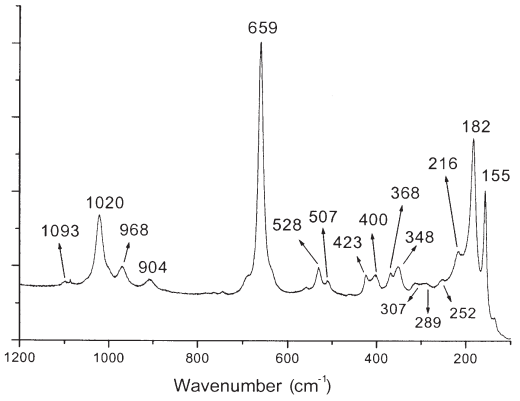

FIG. 6. Raman spectrum obtained from the fibres of amosite represented in Fig. 5*a*.

reveal an homogeneous composition and, according to the nomenclature of the amphiboles proposed by Leake *et al*. (1997), proves to be pure riebeckite (theoretical formula: $Na_2Fe_3^{2+}Fe_2^{3+}[Si_8O_{22}](OH)_2$).

Figure 8 shows a Raman spectrum registered on the fibres shown in Fig. 7*a*; on the whole, the spectrum is richer in bands than the spectra of the other amphiboles studied, probably a consequence of the more complex chemical composition of crocidolite (Table 1). The intense band produced by the ν_{as} vibrations of the Si−O_b−Si groups is shifted here to 1082 cm^{-1}, whereas the intensity of the band at 967 cm^{-1} varies according to the orientation of the fibres with respect to the incident beam. This is strong evidence in favour of assigning the band to the symmetric stretching modes of the O−SiO− groups, rather than to the antisymmetric stretching vibrations as proposed by Lewis *et al*. (1996). The band at 889 cm^{-1} behaves in a similar fashion, and may thus be attributed to the symmetric stretching vibrations of the O−SiO−. The two bands in the spectral region 550−660 – in our case at 664 and 577 cm^{-1} – were ascribed by Lewis *et al*. (1996) to the ν_s modes of Si−O_b−Si bridges, despite the fact that the frequency of the second, at 577 cm^{-1}, is less than expected for the ν_s of the Si−O_b−Si groups (Lazarev, 1972). The structural complexity of the crocidolite, the *A* sites of which are also occupied by Na ions, makes attribution of the bands at low frequencies extremely problematic.

Table 2 allows comparison of the spectrum we obtained and the spectra of the same phase reported by other authors. Our spectrum most

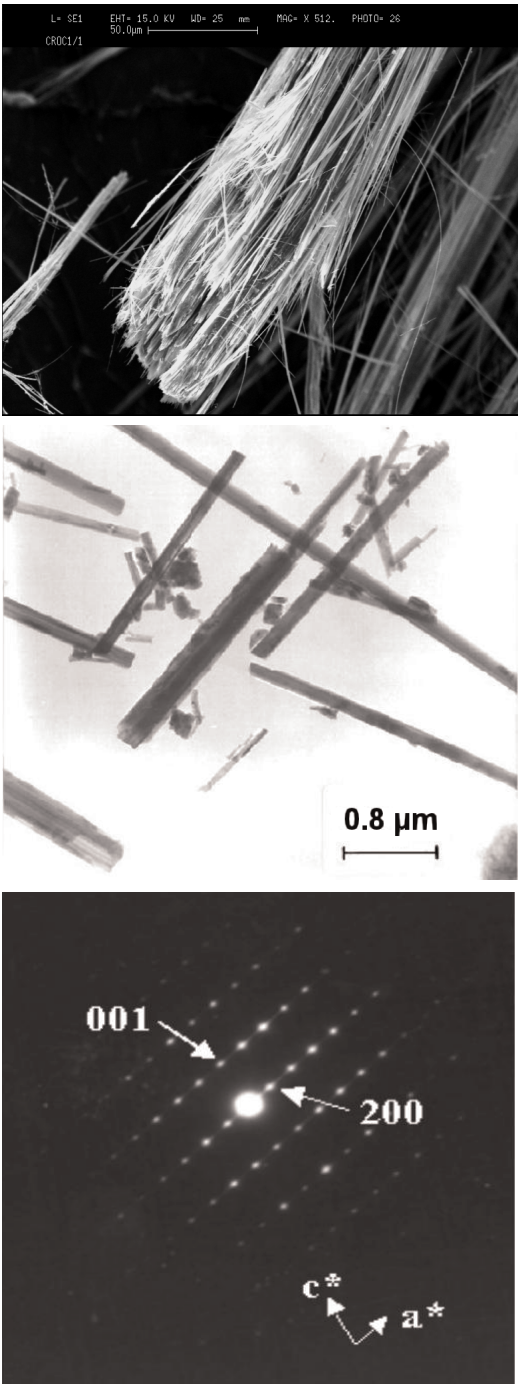

FIG. 7. (*a*) SEM photograph of bundles of crocidolite. (*b*) TEM image of crocidolite fibres. (*c*) SAED pattern from the fibre of crocidolite indicated by the arrow in Fig. 7*b* and seen along the [010] direction.

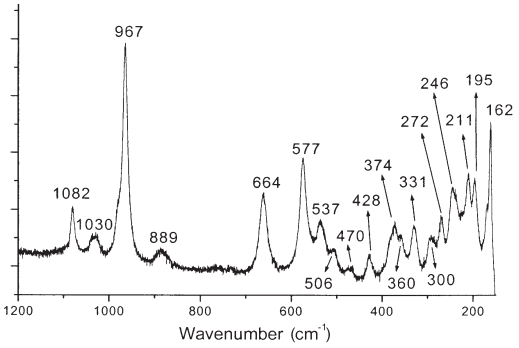

FIG. 8. Raman spectrum of crocidolite obtained from the fibres shown in Fig. 7*a*.

closely matches that of Bard *et al*. (1997); variations in the intensity of several of the bands may be the result of the different angles of the fibres to the incident beam. Turning to the data from Lewis *et al*. (1996), one can observe a shift between their spectrum and ours; moreover, they observe a band of medium intensity at 324 cm^{-1}, which we did not detect. As all of the discrepancies described among the three spectra in Table 2 appear at low frequencies, where vibrations of the cations with different coordination polyhedrons are expected, we can hypothesize that our samples and those of the other authors differ in chemical composition.

Conclusions

The TEM investigations allowed certain identification of the asbestos samples which underwent Raman analyses. The fibre dimensions of the asbestos studied in this work and previously (Rinaudo *et al*., 2003) proved to be dependent on the mineralogical phase: the largest ones are the tremolite fibres and, in decreasing order, those of anthophyllite, amosite, crocidolite and finally, chrysotile.

Comparison of the spectra registered under our experimental conditions with data from the literature lead us to conclude that discrepancies in the band intensities may be related to the orientation of the fibres with respect to the incident beam in the different studies. Other discrepancies in the spectra of the same mineralogical phase and disagreements in the band frequencies may be related to the varying chemical make-up of the mineral phases. In our case, the chemical composition and the mineralogical characteristics of the sample studied by Raman spectroscopy have been defined carefully, to make future comparative studies more fruitful. Raman spectroscopy proved to be a simple and effective technique for distinguishing between all the asbestos phases studied. The vibrational modes of the different Si−O bonds have been proven to vibrate at different frequencies even in mineral phases with similar mineralogical characteristics. Consideration of the frequency of the symmetric stretching modes of the $Si-O_b-Si$ groups allows identification of the mineralogical phase, except in anthophyllite and tremolite where the most important band lies very close (674 and 676 cm^{-1}, respectively). These two minerals can nonetheless be easily distinguished from the region 900−1100 cm^{-1}, where they show distinctly different bands. In fact, the spectral region 900−1100 cm^{-1} allows all the mineralogical phases to be easily identified. These considerations, along with the fact that Raman spectrometry requires only a single bundle of fibres for analysis and no experimental preparation of the samples, indicate that Raman spectroscopy is a useful technique for distinguishing easily between the different mineral phases.

Acknowledgements

The authors wish to thank Dr Martin J. Roe (Macaulay Institute, Craigiebuckler, Aberdeen, Scotland), Dr P.G. Betta of the Azienda Ospedaliera SS. Antonio e Biagio, Alessandria (Italy), Prof. L. Morten of the Dipartimento di Scienze della Terra, Università di Bologna, and the Museo Regionale di Scienze Naturali of Torino, for providing the samples.

References

Bard, D., Yarwood, J. and Tylee, B. (1997) Asbestos fibre identification by Raman microspectroscopy. *Journal of Raman Spectroscopy*, **28**, 803−809.

Blaha, J.J. and Rosasco, G.J. (1978) Raman microprobe spectra of individual microcrystals and fibres of talc, tremolite, and related silicate minerals. *Analytical Chemistry*, **50**, 892−896.

Droop, G.R.T. (1987) A general equation for estimating Fe^{3+} concentrations in ferromagnesian silicates and oxides from microprobe analysis using stoichiometric criteria. *Mineralogical Magazine*, **51**, 431−435.

Farmer, V.C. (1974) *The Infrared Spectra of Minerals*. Monograph **4**, Mineralogical Society, London.

Frost, R.L. (1995) Fourier transform Raman spectro-

scopy of kaolinite, dickite and halloysite. *Clays and Clay Minerals*, **43**, 191–195.

Frost, R.L. (1997) The structure of the kaolinite minerals – a FT-Raman study. *Clay Minerals*, **32**, 65–77.

Frost, R.L. and Kristof, J. (1997) Intercalation of halloysite: a Raman spectroscopic study. *Clays and Clay Minerals* **45**, 551–563.

Kloprogge, J.T., Frost, R.L. and Rintoul, L. (1999) Single crystal Raman microscopic study of the asbestos mineral chrysotile. *Physical Chemistry Chemical Physics*, **1**, 2559–2564.

Kloprogge, J.T., Case, M.H. and Frost, R.L. (2001) Raman microscopic study of the Li amphibole holmquistite, from the Mertin Marietta Quarry, Bessemer City, NC, USA. *Mineralogical Magazine*, **65**, 775–785.

Lazarev, A.N. (1972) *Vibrational Spectra and Structure of Silicates*. Consultants Bureau, New York and London, p. 1.

Leake, B.E., Woolley, A.R., Arps, C.E.S., Birch, W.D., Gilbert, M.C., Grice, J.D., Hawthorne, F.C., Kato, A., Kisch, H.J., Krivovichev, V.G., Linthout, K., Laird, J., Mandarino, J.A., Maresch, W.V., Nickel, E.H., Rock, N.M.S., Schumacher, J.C., Smith, D.C., Stephenson, N.C.N., Ungaretti, L., Whittaker, E.J.W. and Youzhi, G. (1997) Nomenclature of amphiboles: report of the subcommittee on amphiboles of the International Mineralogical Association, Commission on New Minerals and Mineral Names. *Mineralogical Magazine*, **61**, 295–321.

Lewis, I.R., Chaffin, N.C., Gunter, M.E. and Griffiths, P.R. (1996) Vibrational spectroscopic studies of asbestos and comparison of suitability for remote analysis. *Spectrochimica Acta A*, **52**, 315–328.

Rinaudo, C., Gastaldi D. and Belluso, E. (2003) Characterization of chrysotile, antigorite and lizardite by FT-Raman Spectroscopy. *The Canadian Mineralogist*, **41**, 883–890.

Yavuz, F. (1999) A revised program for microprobe-derived amphibole analyses using the IMA rules. *Computers & Geosciences*, **25**, 909–927.

[*Manuscript received 11 September 2003: revised 16 December 2003*]